Finite Element Model of Shape Memory Alloy Incorporating Drucker-Prager Model

Yan Tingjun*[1], Zhao Linna[2]
[1,2]Department of Chemical process machinery, Beijing University of Chemical Technology
No.15 east street of North Third Road, Chaoyang District, Beijing, China,
[1]Ph.: +86-13501098179; [2]Ph.: +86-13811385276
Corresponding author, e-mail: yantj555@163.com[1], zhaolinna24@163.com

Abstract
The unique features of shape memory alloys (SMA), including pseudoelasticity and shape memory effect, give SMAs a wide application in aeronautical, biomedical, and structural engineering. These features stimulate the interest in the development of constitutive models. In this paper, a 3D finite element model of shape memory alloy material model has been developed to incorporate the Drucker – Prager model in order to describe the asymmetry of SMA under tension and compression. This paper also takes into account the variation of Young's modulus of the austenite and the martensite. The development and implementation of a robust integration algorithm is presented. The provided numerical simulation demonstrates its capabilities. Further studies should be performed to seek quantitative fitting with experimental results.

Keywords: shape memory alloy; Drucker-Prager model; finite element model

1. Introduction

The shape memory alloys (SMAs) have unique characteristics that remember an original ability. At the microscopic level, SMAs present two different crystallographic structures, one characterized by austenite (A) and another one by martensite (M). The reversible martensitic phase transformation results in two unique effects: the pseudoelasticity (PE) and the shape memory effect (SME) [1, 2]. In Figure 1a, whenever σ is positive, the specimen completely returns to its original shape with stress-free configuration. Thus the material is named PE. In Figure 1b, after unloaded to a stress-free state, residual strains can be observed. However, if the material is heated, the specimen eventually returns to the original point A. Therefore, the material undergoes an inverse transformation process, which is called SME.

Due to these unique features (PE and SME), SMA has been applied successfully in many different fields such as aeronautical, biomedical, and structural engineering. The commercial applications of SMA have stimulated wide interest in the development of accurate constitutive models to catch the basic material behavior [3, 4]. Until now, many 1D models [5-8] and 3D models [9-10] have been available. Out of these material models, the 3D model proposed by Souza et al. [9] is very attractive because of its ability to reproduce all the main features relative to shape memory materials in a 3D model. Auricchio later improved this model with a Prager-type limit function to catch the characteristic asymmetrical behavior of SMA during a tension-compression test [10]. However, the Drucker-Prager Model is much more widely used than the Prager-type limit function to define asymmetry. Moreover, the austenite and the martensite have a different elastic modulus [11-13]. Thus, the goals of this work are to reproduce PE and SME features of shape memory alloy and to cover asymmetric behavior in tension and compression with the Drucker–Prager model, as well as variation of elastic modulus of the austenite and martensite.

3916 ■

e-ISSN: 2087-278X
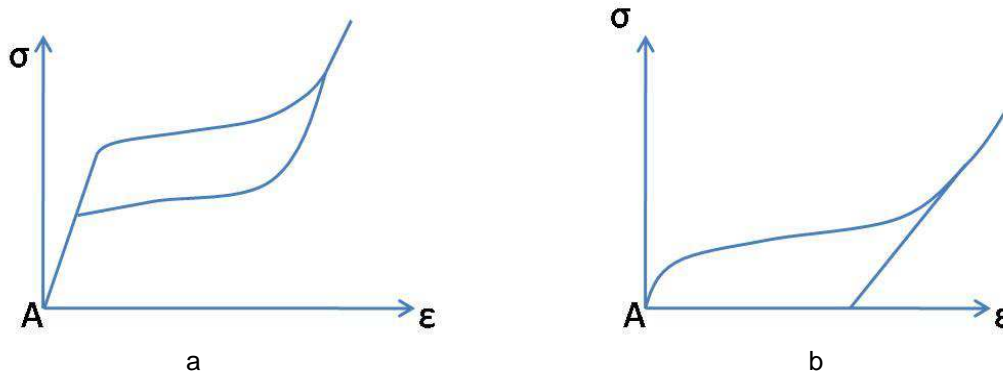
Figure 1. a. Pseudoelasticity; b. Shape Memory effect

2. The Shape Memory Material Model

At first, we define a second-order tensor, $\mathbf{E}_t$, as transformation strain to measure the strain associated with the phase transformation, particularly with the conversion from austenite or multiple – variant martensite to the single variant martensite. Thus,

$$0 \leq \|\mathbf{E}_t\| \leq \epsilon_L \tag{1}$$

ϵ_L is a maximum value of Norm of $\mathbf{E}_t$ in the phase transformation, in which the material is fully transformed.

Therefore, the stress, σ, is expressed in terms of strain:

$$\sigma = \mathbb{L} : (\mathbf{E} - \mathbf{E}_t) \tag{2}$$

regarding that variation of the elastic modulus of the austenite and martensite, we assume that $\mathbb{L}$ is a linear function of the norm of $\mathbf{E}_t$:

$$\mathbb{L} = \frac{\|\mathbf{E}_t\|}{\epsilon_L}(\mathbb{L}_M - \mathbb{L}_A) + \mathbb{L}_A \tag{3}$$

When the material is in its parent phase, $\mathbb{L} = \mathbb{L}_A$; when the material is in its product phase, $\mathbb{L} = \mathbb{L}_M$. Here the double-struck font refers to the fourth order tensor.

For convenience, we split the stress as follows:

$$\sigma = \sigma' + \mathbf{1}p \tag{4}$$

where σ' is the deviatoric component of σ, and p is the trace of σ.

During the transformation, the transformation stress is defined as [9]

$$\mathbf{X}_t = \sigma' - \frac{[\tau_M(T) + h\|\mathbf{E}_t\|]\mathbf{E}_t'}{\|\mathbf{E}_t'\|} \tag{5}$$

where $\tau_M(T) = (\beta(T - T_0))^+$ is a positive and monotonically increasing function of the room temperature T, and the material dependent temperature T_0 below which no twinned martensite occurs. β is a material parameter. h is a material parameter associated with the hardening of the material during the phase transformation.

The evolutionary equation for $\mathbf{E}_t$ has the following form:

$$\mathbf{E}_t = \mathbf{E}_t\,(n) + \Delta\xi\,\frac{\partial F}{\partial\sigma} \tag{6}$$

where the limit function F is given in terms of the transformation stress $\mathbf{X}_t$ and the elastic domain radius R in form of the Drucker-Prager type

$$F(\mathbf{X}_t,\mathbf{p}) = \|\mathbf{X}_t\| \pm 3\alpha p - R \tag{7}$$

where α is material parameter that characterizes the difference between compression and tension.

In the loading stage,

$$F(\mathbf{X}_t,\mathbf{p}) = \|\mathbf{X}_t\| + 3\alpha p - R \tag{8}$$

In the unloading stage,

$$F(\mathbf{X}_t,\mathbf{p}) = \|\mathbf{X}_t\| - 3\alpha p - R \tag{9}$$

In the program, the energy increment is computed to judge the loading stage and unloading stage.

Figure 2 illustrates the above flow rule. The flow occurs along the boundaries ($F=0$), while the interior part represents the elastic behavior.

Thus, we have the following equations to describe the phase transformation.

$$\begin{cases} \sigma = \mathbb{L}:(\mathbf{E} - \mathbf{E}_t) \\ \mathbf{X}_t = \sigma' - \dfrac{\left[\tau_M(T) + h\|\mathbf{E}_t\|\right]\mathbf{E}_t'}{\|\mathbf{E}_t'\|} \\ \mathbf{E}_t = \mathbf{E}_t\,(n) + \Delta\xi\,\dfrac{\partial F}{\partial\sigma} \\ \|\mathbf{E}_t\| \le \epsilon_L \\ F(\mathbf{X}_t) = \|\mathbf{X}_t\| \pm 3\alpha p - R \le 0 \\ \Delta\xi \ge 0 \quad \Delta\xi F(\mathbf{X}_t) = 0 \end{cases} \tag{10}$$

The last equation in Eq. (10) is the classical Kuhn-Tucker conditions to reduce the problem as a constrained optimization problem.
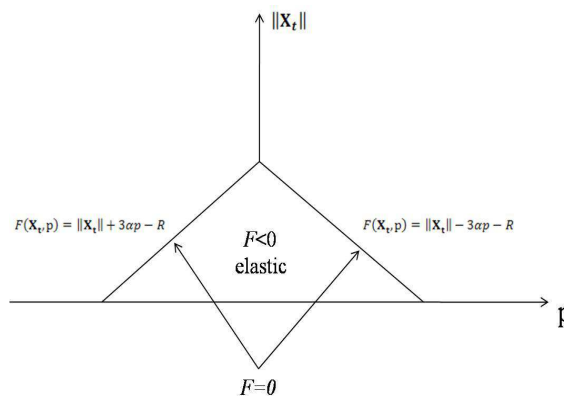
Figure 2. Flow rule for inelastic potential

---

3. Research Method
3.1. Parameters Determined by Uniaxial Test

Figure 3 illustrates the variation of stresses with strain in the uniaxial test, which can be used to determine such parameters as $\mathbb{L}_A$, $\mathbb{L}_M$, β, T_0, ϵ_L, h, and R.

(1) $\mathbb{L}_A$ and $\mathbb{L}_M$ can be defined by lines OA and BC, assuming they are linear elastic.
(2) ϵ_L can be determined in Figure 3.
(3) The onset of phase transformation occurs at A. Thus,

$$\sqrt{\left(\frac{2}{3}\right)(\sigma_A - \beta(T - T_0))} + \alpha\sigma_A = R \tag{11}$$

Similarly, at E,

$$\sqrt{\left(\frac{2}{3}\right)(\beta(T - T_0) - \sigma_E)} + \alpha\sigma_E = R \tag{12}$$

When we have multiple uniaxial tests with different temperatures $T=T_1$, and $T=T_2$ respectively, we may determine β, T_0 and R.
(4) At B,

$$\sqrt{\left(\frac{2}{3}\right)(\sigma_B - \beta(T - T_0) - h\epsilon_L)} + \alpha\sigma_B = R \tag{13}$$

Therefore, h is defined when R, β, T_0, ϵ_L are known.
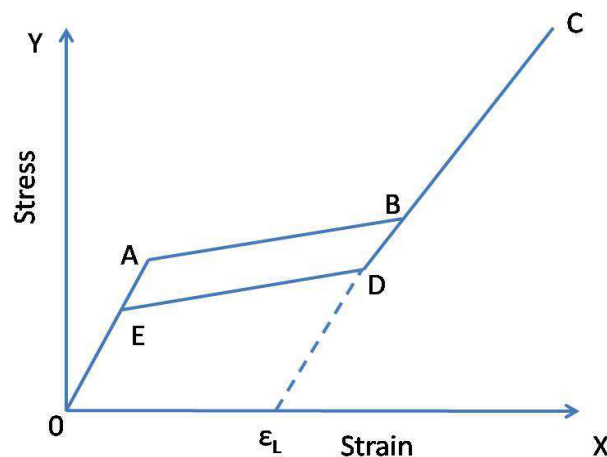
Figure 3. Typical uniaxial test of SMA

3.2. Numerical Aspects

The phase transformation is divided into three stages: onset transformation, transformation, and saturated transformation.
(1) Onset of transformation

The onset of transformation occurs when $F > 0$, $\|\mathbf{E}_t\| = 0$ and $\mathbb{L} = \dfrac{\|\mathbf{E}_t\|}{\epsilon_L}(\mathbb{L}_M - \mathbb{L}_A) + \mathbb{L}_A$. Therefore,

$$\frac{\partial F}{\partial \sigma} = \frac{\mathbf{X}_t}{\|\mathbf{X}_t\|} + \alpha \mathbf{I} = N(\mathbf{X}_t) + \alpha \mathbf{I} \tag{14}$$

The governing equation in this stage is written as

$$\begin{cases} \mathbf{X}_t - \sigma' + [\tau_M(T) + Hz_\sigma]\dfrac{\sigma'}{\|\sigma'\|} = 0 \\ z_\sigma - \|\mathbf{E}_t'\| = 0 \\ \|\mathbf{X}_t\| + 3\alpha p - R = 0 \\ \mathbf{E}_t - \Delta d_t \, \mathbb{I}\big(N(\mathbf{X}]_t) + \alpha \mathbf{I}\big) = 0 \end{cases} \tag{15}$$

With unknowns $\{\mathbf{X}_t \quad z_\sigma \quad \Delta d_{tr} \quad \mathbf{E}_t\}$

$$[D] = \begin{bmatrix} \mathbf{I} & H \cdot N(\sigma') & 0 & G\mathbb{B}(\sigma')[(\mathbf{I}]'\mathbb{L} - \mathbf{I}'\mathbb{C}) + \mathbf{I}'\mathbb{L} - \mathbf{I}'\mathbb{C}] \\ 0 & 1 & 0 & -N(\mathbf{E}_t') \\ N(\mathbf{X}_t) & 0 & 0 & -\alpha \mathbf{I}\mathbb{L} + \alpha \mathbf{I}\mathbb{C} \\ -\Delta d_{tr}\mathbb{B}(\mathbf{X}_t) & 0 & -[N(\mathbf{X}]_t) - \alpha \mathbf{I} & \mathbf{I} \end{bmatrix} \tag{16}$$

$$G = \tau_M(T) + Hz_\sigma \tag{17}$$

$$\mathbb{C} = (\mathbb{L}_M - \mathbb{L}_A):(\mathbf{E} - \mathbf{E}_t) \otimes \frac{N(\mathbf{E}_t)}{\varepsilon_L} \tag{18}$$

The consistent tangent tensor has the following form with unknowns $\{\mathbf{X}_t \quad z_\sigma \quad \Delta d_t \quad \mathbf{E}_t \quad \mathbf{E}\}$

$$\begin{bmatrix} \mathbf{I} & H \cdot N(\sigma') & 0 & G\mathbb{B}(\sigma')[(\mathbf{I}]'\mathbb{L} - \mathbf{I}'\mathbb{C}) + \mathbf{I}'\mathbb{L} - \mathbf{I}'\mathbb{C}] \\ 0 & 1 & 0 & -N(\mathbf{E}_t') \\ N(\mathbf{X}_t) & 0 & 0 & -\alpha \mathbf{I}\mathbb{L} + \alpha \mathbf{I}\mathbb{C} \\ -\Delta d_t\mathbb{B}(\mathbf{X}_t) & 0 & -[N(\mathbf{X}]_t) - \alpha \mathbf{I} & \mathbf{I} \end{bmatrix} \begin{Bmatrix} d\mathbf{X}_t \\ dz_\sigma \\ d\Delta d_t \\ d\mathbf{E}_t \end{Bmatrix} + \begin{Bmatrix} -\mathbf{I}'\mathbb{L} \\ 0 \\ \alpha \mathbf{I}\mathbb{L} \\ 0 \end{Bmatrix} d\mathbf{E} = 0 \tag{19}$$

$$\begin{Bmatrix} d\mathbf{X}_t \\ dz_\sigma \\ d\Delta d_t \\ d\mathbf{E}_t \end{Bmatrix} = \begin{bmatrix} \mathbf{I} & H \cdot N(\sigma') & 0 & G\mathbb{B}(\sigma')[(\mathbf{I}]'\mathbb{L} - \mathbf{I}'\mathbb{C}) + \mathbf{I}'\mathbb{L} - \mathbf{I}'\mathbb{C}] \\ 0 & 1 & 0 & -N(\mathbf{E}_t') \\ N(\mathbf{X}_t) & 0 & 0 & -\alpha \mathbf{I}\mathbb{L} + \alpha \mathbf{I}\mathbb{C} \\ -\Delta d_t\mathbb{B}(\mathbf{X}_t) & 0 & -[N(\mathbf{X}]_t) - \alpha \mathbf{I} & \mathbf{I} \end{bmatrix}^{-1} \begin{Bmatrix} \mathbf{I}'\mathbb{L} \\ 0 \\ -\alpha \mathbf{I}\mathbb{L} \\ 0 \end{Bmatrix} d\mathbf{E} \tag{20}$$

The relation between $d\mathbf{E}_t$ and $d\mathbf{E}$ can be written in the form

$$d\mathbf{E}_t = \mathbb{A}:d\mathbf{E} \tag{21}$$

where $\mathbb{A}$ is determined by Eq. (20).
By substituting the above equation into the following equation,

$$d\sigma = \mathbb{L}:(d\mathbf{E} - d\mathbf{E}_t) + \mathbb{C}:d\mathbf{E}_t \tag{22}$$

we have,

$$\frac{d\sigma}{dE} = \mathbb{L} + (\mathbb{C} - \mathbb{L}):\mathbb{A} \tag{23}$$

(2) Transformation stage

The transformation stage occurs when F > 0, $0 < \|E_t\| < \epsilon_L$, and $\mathbb{L} = \frac{\|E_t\|}{\epsilon_L}(\mathbb{L}_M - \mathbb{L}_A) + \mathbb{L}_A$. Therefore,

$$\frac{\partial F}{\partial \sigma} = \frac{X_{tr}}{\|X_{tr}\|} + \alpha I = N(X_t) + \alpha I \tag{24}$$

The governing equation in this stage is written as

$$\begin{cases} X_t - \sigma' + \left[\frac{\tau_M(T)}{z_\sigma} + H\right]E_t' = 0 \\ z_\sigma - \|E_t'\| = 0 \\ \|X_t\| \pm 3\alpha p - R = 0 \\ E_t - E_t(n) - \Delta d_t \left[(N(X]_t) \pm \alpha I\right) = 0 \end{cases} \tag{25}$$

In the case of loading and unloading, α is positive and negative, respectively. With unknowns $\{X_t \quad z_\sigma \quad \Delta d_t \quad E_t\}$

$$[D] = \begin{bmatrix} \mathbb{I} & \dfrac{-\tau_M(T)}{z_\sigma^2 E_t'} & 0 & G\dfrac{\square'}{z_\sigma \mathbb{I}} + \mathbb{I}'\mathbb{L} - \mathbb{I}'\mathbb{C} \\ 0 & 1 & 0 & -N(E_t') \\ N(X_t) & 0 & 0 & \mp\alpha\mathbb{I}\mathbb{L} \pm \alpha\mathbb{I}\mathbb{C} \\ -\Delta d_t \mathbb{B}(X_t) & 0 & -[N(X]_t) \mp \alpha I & \mathbb{I} \end{bmatrix} \tag{26}$$

Similar to the onset phase, we have,

$$\frac{d\sigma}{dE} = \mathbb{L} + (\mathbb{C} - \mathbb{L}):\mathbb{A} \tag{27}$$

(3) Saturated Phase

In the saturated phase of transformation, we assume E_t has no change. Therefore, the stress is computed by

$$[\sigma = \mathbb{L}_M(E - E]_t) \tag{28}$$

and the consistent tangent matrix is computed as

$$\frac{d\sigma}{dE} = \mathbb{L}_M \tag{29}$$

(4) Computation Procedure in the Phase Transformation
Computation of the phase transformation goes through the following steps:
1) Elastic stress predictor: $\sigma^{trial} = \mathbb{L}:(E - E_t)$
2) Check for transformation. $(0 < \|E_t t\| < \epsilon_L; \|X_t t\| \pm 3\alpha p - R > 0)$
3) No: Elastic step: $\sigma = \sigma^{trial} \quad E_t = E_t$

4) Yes: Iteration for γ　Δd_t　$\mathbf{E}_t$
5) After phase transformation, check $\|\mathbf{E}_t\| > \epsilon_L$.
6) Yes: Go to saturated phase transformation computation.
7) No: Update stresses and compute consistent tangent matrix.

4. Results and Discussion

We applied the presented model to reproduce the basic SMA features through numerical tests that consider a material with the following properties.

Young's modulus of the austenite and the martensite:

EA=90,000MPa, EM=60,000MPa, Poisson's ratio: v=0.30

Other parameters for the phase transformation:

R=40MPa, h=600MPa, β=8.5MPa K^{-1}, T_0=250.0K, $\epsilon_L = 0.035$, α=0.05

Using a body temperature of T=280.0K, we performed uniaxial isothermal loading. The simulation results are plotted in Figure 4. In the loading part, SMA goes through the elastic stage, phase transformation, and saturated phase transformation. While unloading, SMA reverses the path back to original point, which shows the PE feature. Please also note that the stress at A is 388.7MPa, and -439.5MPa at B, which demonstrates the asymmetry between tension and compression. Furthermore, the difference in the Young's modulus at A and B is in accordance with the given material properties (EA=90,000MPa, EM=60,000MPa).
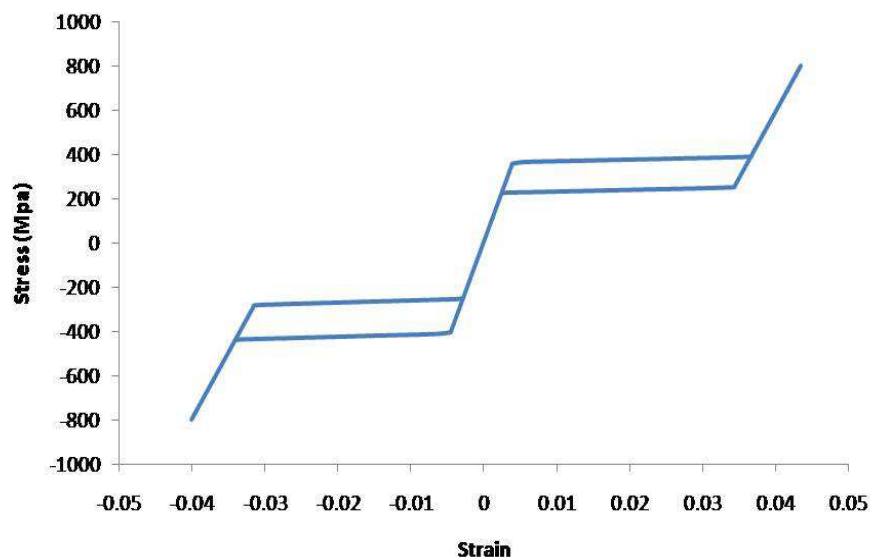
Figure 4. Stress vs strain under uniaxial loading

In order to reproduce shape memory effect, we used the following three steps to conduct the uniaxial test:
1)　Isothermal stress-driven loading (T=250.0K), up to 200MPa.
2)　Unload back to a stress-free state.
3)　Then, increase the temperature up to 257.50K.

Figure 5 illustrates that SMA, while loaded to 200MPa, reaches the saturated stage. After unloaded to a free-stress state, a residual strain remains. In the third step, with heating to temperature 257.50K, the residual strain disappears and SMA returns to the original form, which proves shape memory effect.
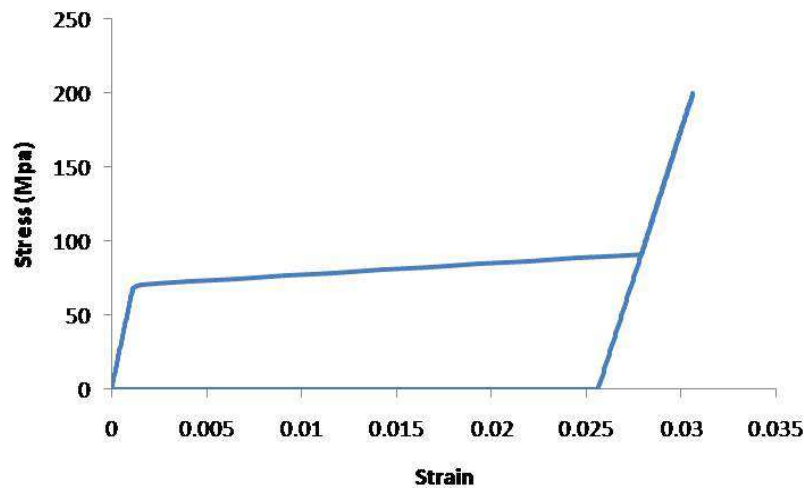
Figure 5. Shape memory effect

Finally, with the above material properties, we simulated the perforated square model (Figure 6) under two different body temperatures (T=250K, and T=280K). The vertical direction is under tension to strain 0.01 and then returns to zero. Because of its symmetry, we selected one-quarter for the study.
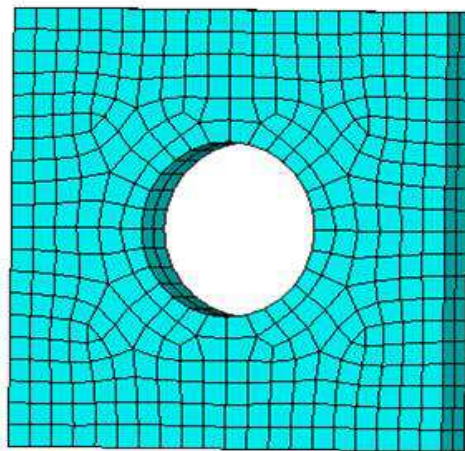
Figure 6. Perforated square model

Figure 8 illustrates the strains and stresses of the model with T=280K in the whole process. In the loading stage, the stresses and strains increase to maximum value 717MPa and 0.05, respectively. However, after unloading, they decrease to near zero. The results are different for T=250K (Figure 7). After unloading, the model has remaining stresses and strains with a maximum stress approximately 100MPa and a maximum strain 0.015. It states SMA has different stress-strain relation under different temperatures, which is consistent with results in Figures 4 and 5.

(a). loading, stress contour (MPa)

(b). loading, inelastic strain contour

(c) unloading, stress contour (MPa)

(d) unloading, inelastic strain contour
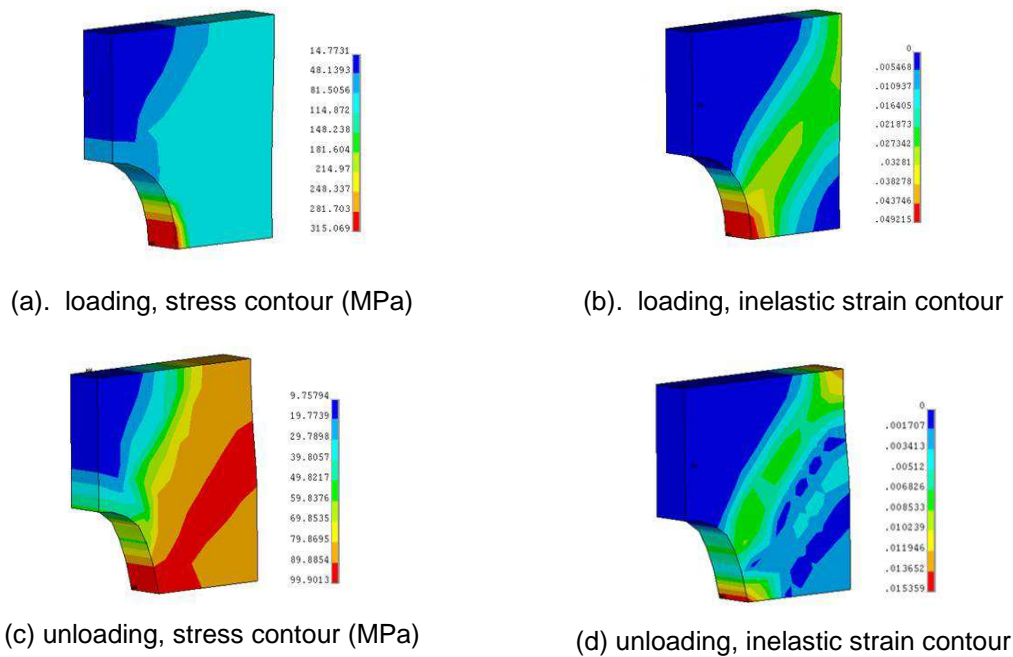
Figure 7. Stress and inelastic strain contour T=250K

(a) loading, stress contour (MPa)

(b) loading, inelastic strain contour

(c) unloading, stress contour (MPa)

(d) unloading, inelastic strain contour
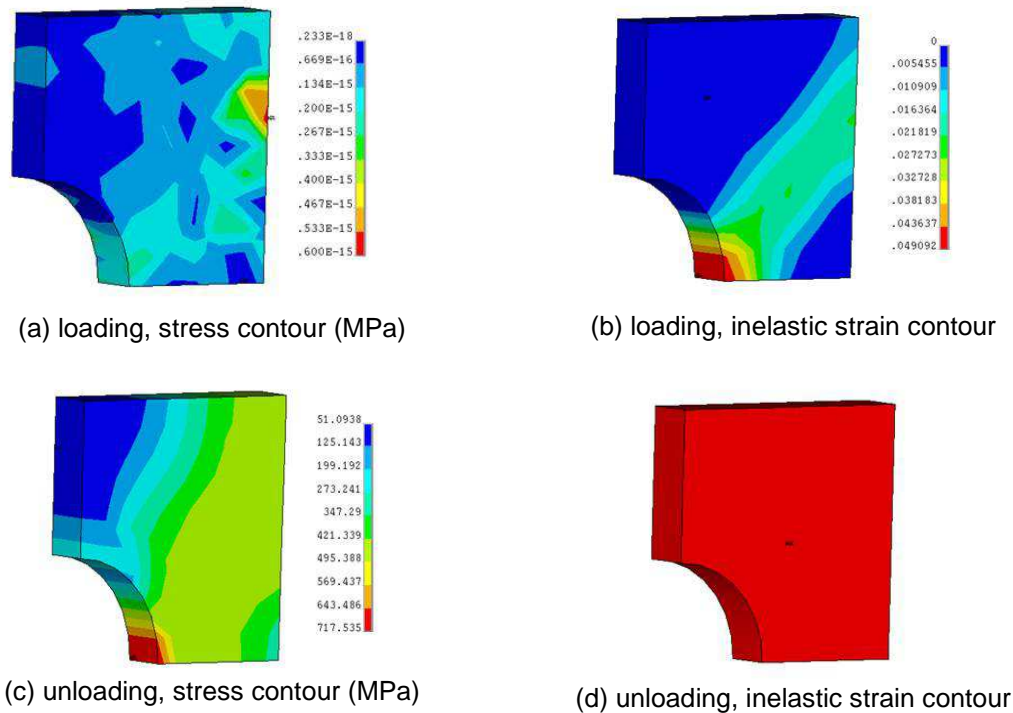
Figure 8. Stress and inelastic strain contour T=280K

5. Conclusion

We propose a new model for the description of pseudoelastic behavior and shape memory alloy effect in a 3D setting. The new model incorporates the SMA model with the Drucker-Prager model to describe asymmetry between tension and compression. Moreover, we take into account the variation of Young's modulus of the austenite and the martensite. We

provide numerical simulations to illustrate the capabilities of the model at hand. Further studies should be performed to seek quantitative fitting with experimental results.

References

[1] Funakubo H. Shape Memory Alloys. G*ordon and Breach Science Publishers*. 1987; 16(1): 122-131.
[2] Fremond M. A Thermomechanical model in Free Boundary Problems. *Theory and Applications*. 1990; 24(1): 295-306.
[3] Auricchio, Sacco. A temperature-driven beam for shape-memory alloys: constitutive modelling, finite-element implementation and numerical simulations. *Computer Methods in Applied Mechanics and Engineering*. 1999; 174: 171-190.
[4] Auricchio F. A robust integration-algorithm for a finite-strain shape memory-alloy superelastic model. *International Journal of Plasticity*. 2001; 17: 971-990.
[5] Liang C, Rogers CA. One-dimensional thermomechanical constitutive relations for shape memory materials. *Journal of Intelligent Materials Systems and Structures*. 1990; 1: 207-234.
[6] Graesser EJ, Cozzarelli FA. Shape memory alloys as new materials for aseismic isolation. *Journal of Engineering Mechanics (ASCE)*. 2011; 117: 2590-2608.
[7] Brinson LC. One-dimensional constitutive behavior of shape memory alloys: thermomechanical derivation with non-constant material functions and redefined martensite internal variables. *Journal of Intelligent Materials Systems and Structures*. 1993; 4: 229-242.
[8] Abeyaratne R, Kim, SJ, Knowles, JK. A one-dimensional continuum model for shape-memory alloys. *International Journal of Solids and Structures*. 1994; 31: 2229-2249.
[9] Souza AC, Mamiya EN, Zouain N. Three-dimensional model for solids undergoing stress-induced phase transformations. *European Journal of Mechanics-A/Solids*. 1998; 17: 789-806.
[10] Auricchio F, Petrini L. Improvements and algorithmical considerations on a recent three-dimensional model describing stress-induced solid phase transformations. *International Journal for Numerical Methods in Engineering*. 2002; 55: 1255-1284.
[11] Yao Baoguo, Yan Lixia, Wang Jianchao, Hong Shuiyuan. Mechanical Theorem Proving in Geometry. *TELKOMNIKA Indonesian Journal of Electrical Engineering*. 2012; 10(7): 1554-1559.
[12] Ye junjian, Zhang Qin, Zuo Yujun, Cheng Wei. Digital-image Based Numerical Simulation on Failure Process of High-sulfur Coal. *TELKOMNIKA Indonesian Journal of Electrical Engineering*. 2013; 11(1): 203-212.
[13] Wang Yu, Wu Hao, Sheng Zhenyu. A Prioritized Test Generation Method For Pair-wise Testing. *TELKOMNIKA Indonesian Journal of Electrical Engineering*. 2013; 11(1): 136-143.